Practical expressions for local magnetic shear, normal and geodesic curvatures in an axisymmetric plasma equilibrium of arbitrary cross-section.

P.J. Mc Carthy

Department of Physics, University College Cork, Association Euratom-DCU, Cork, Ireland

E-mail: pjm@ucc.ie

ASDEX Upgrade Team

Max Planck Institut für Plasmaphysik, Euratom Association, Boltzmannstrasse 2, D-85748 Garching, Germany

Abstract.
We present practical expressions involving the toroidal field and the poloidal flux that describe without approximation the local magnetic shear and normal and geodesic curvatures in an axisymmetric plasma equilibrium of arbitrary cross-sectional geometry. Experimental examples from the ASDEX Upgrade tokamak indicate that a zero crossing of both local shear and poloidal current density in the outboard pedestal region first occurs with the appearance of ELMs.

(Figures in this article are in colour only in the electronic version)

1. Introduction

Local magnetic shear, which is a measure of the rate at which initially adjacent field lines on neighbouring flux surface separate with distance advanced along the field lines, is a structural property of magnetic fields that has an important influence on plasma stability. There are two somewhat different definitions of local magnetic shear in the literature. Greene and Chance [2] and others, e.g. [3], citing Greene and Johnson [1], define local shear as

$$S_\ell^{\,G} = \frac{\boldsymbol{B}\times\nabla\psi}{|\nabla\psi|^2}\cdot\nabla\times\frac{\boldsymbol{B}\times\nabla\psi}{|\nabla\psi|^2} \tag{1}$$

More recently, Nadeem *et al.* [4] introduced the definition

$$S_\ell^{\,N} = 2\pi\,\boldsymbol{e}_\perp\cdot\nabla\times\boldsymbol{e}_\perp \tag{2}$$

where the unit vector $\boldsymbol{e}_\perp$ is perpendicular to the local magnetic field direction $\boldsymbol{b}=\boldsymbol{B}/B$ and lies in the flux surface. It is given by the expression

$$\boldsymbol{e}_\perp = \boldsymbol{e}_\psi\times\boldsymbol{b} = \frac{\nabla\psi}{|\nabla\psi|}\times\frac{\boldsymbol{B}}{B} \tag{3}$$

where $\boldsymbol{e}_\psi$ is the unit normal to the flux surface. Note $S_\ell^{\,N}$ has the dimensions of inverse length. Writing equation (1) as $\boldsymbol{g}\cdot\nabla\times\boldsymbol{g}$ with

$$\boldsymbol{g} = \frac{\boldsymbol{B}\times\nabla\psi}{|\nabla\psi|^2} \equiv \frac{\boldsymbol{B}}{|\nabla\psi|}\times\boldsymbol{e}_\psi \tag{4}$$

it is seen that both definitions are similar (although differently dimensioned), however $\boldsymbol{g}$ has the disadvantage of being unbounded at the magnetic axis and on saddle points and we accordingly work with definition (2) which is slightly altered here to:

$$S_\ell = -\boldsymbol{e}_\perp\cdot\nabla\times\boldsymbol{e}_\perp \tag{5}$$

We choose to omit the factor of 2π, while the change of sign is consistent with calculating the poloidal flux at (R,Z) as the flux through the horizontal disk of radius R centred on $R=0$ and passing through (R,Z). In [4], the integration is carried out from the magnetic axis to the flux surface.

In the next section, after first presenting a physical interpretation for (5), we proceed to derive a general expression for the local shear involving only standard quantities routinely available from an axisymmetric equilibrium code, namely the toroidal field and the poloidal flux. Similar expressions are derived for the components of the magnetic field line curvature. In section 3 we give numerical examples using ASDEX Upgrade experimental data which indicate that local shear reversal takes place in the outboard pedestal region with the appearance of the first ELM and this also correlates with a zero crossing of the poloidal current density. A summary and some concluding remarks follow in the final section.

2. Derivation of expressions for local shear and normal and geodesic curvature in terms of ψ and F

2.1. Local shear

We now give a physical interpretation for S_ℓ as given by equation (5) by first relating it to a widely used conventional expression for shear.

Consider a large aspect ratio plasma, $R/a \gg 1$ (R and a are the major and minor radii) with circular flux surfaces of radius $r \leq a$ where the safety factor profile $q(r)$ depends only on r. It is shown in Appendix A of [4] that equation (5) in this case simplifies to

$$S_\ell \approx \left(\frac{B_0}{Bq}\right)^2 \frac{r}{R}\frac{dq}{dr}\left(1 - \frac{r}{R}\cos\theta\right) \tag{6}$$

where B_0 is the toroidal magnetic field B_ϕ at the plasma centre and $B = \sqrt{B_\phi^2 + B_\theta^2}$ is the total field (B_θ is the poloidal field magnitude). For $a/R \ll 1$ and $q(r) = rB_\phi/(RB_\theta)$ equal to unity or greater, it follows that $B_\theta/B_\phi \leq r/R \ll 1$ and hence $B_\phi/B \to 1$ in the limit $a/R \to 0$ and expression (6) simplifies to

$$S_\ell = \frac{1}{qR}\frac{r}{q}\frac{dq}{dr} \equiv \frac{s}{qR} \tag{7}$$

where $s = (r/q)dq/dr$ is the widely used dimensionless global shear parameter valid in the limit of infinite aspect ratio circular plasmas.

For this simplified geometry, the change in poloidal angle $\Delta\theta$ corresponding to a toroidal advance of $\Delta\phi$ radians is given by $\Delta\theta \equiv \Delta\theta(r) = \Delta\phi/q(r)$ at radius r. For a neighbouring flux surface at radius $r + \delta r$ the corresponding change in θ is $\Delta\theta(r + \delta\, r) = \Delta\phi/q(r + \delta r) = \Delta\theta/(1 + (\delta r/q)dq/dr)$ to first order in δr. Hence the poloidal separation $\delta h = r\,\delta\theta$ of two field lines initially at the same poloidal and toroidal angular locations (θ, ϕ) on neighbouring flux surfaces at radii r and $r + \delta r$ following an advance through a toroidal angle of $q\,\Delta\theta$ radians, to first order in δr, is given by $\delta h = -\Delta\theta\,\delta r(r/q)dq/dr = -\Delta\theta\,\delta r\, s$ where $s = (r/q)dq/dr$ is the conventional dimensionless shear parameter. Thus $s = -(\delta h/\delta r)/\Delta\theta$ is the poloidal separation per unit radial separation of the flux surfaces for unit angular poloidal advance $\Delta\theta = 1$ radian, corresponding to $\Delta\phi = q$ radians, or equivalently for travelling a distance $\Delta L \approx qR$ along the field line ($\Delta L = qR$ is exact in the limit $a/R \to 0$). Since local and global parameters are identical in this high symmetry case, the local shear, here given by $S_\ell = s/qR$, can be interpreted as *the differential field line separation per unit distance along the field line* (where here "differential" is shorthand for "per unit radial separation of neighbouring surfaces"). Evaluation of the cross product (3) in cylindrical coordinates (R, ϕ, Z) where $R\boldsymbol{B}_\theta = (-\psi_Z,\, 0,\, \psi_R)$ and $\psi_Z = \partial\psi/\partial Z$, etc. yields

$$\boldsymbol{e}_\perp = \left(\frac{-F\psi_Z}{RB|\nabla\psi|},\ \frac{-|\nabla\psi|}{RB},\ \frac{F\psi_R}{RB|\nabla\psi|}\right) \tag{8}$$

where $F(\psi) = RB_\phi$ and $\psi \equiv \psi_{pol}/(2\pi)$ is the poloidal flux per radian.

Evaluation of $S_\ell = -\boldsymbol{e}_\perp \cdot \nabla \times \boldsymbol{e}_\perp$ leads to the following compact expression, obtained with the help of *Mathematica*[5] :

$$S_\ell = \frac{F}{R^4 B_\theta^2 B^2}\left\{(\psi_{RR} - \psi_{ZZ})(\psi_R^2 - \psi_Z^2) + 4\psi_R \psi_Z \psi_{RZ}\right\} + \frac{F\psi_R}{R^3 B^2} - \frac{F' B_\theta^2}{B^2}. \tag{9}$$

This exact expression for the local magnetic shear, valid for an axisymmetric MHD equilibrium of arbitrary poloidal cross-section and aspect ratio, is expressed in terms of standard equilibrium code outputs, namely the toroidal magnetic field B_ϕ, the flux surface quantity $F' = d(RB_\phi)/d\psi$ and spatial derivatives of the poloidal flux $2\pi\psi$ (including the squared modulus of the poloidal field $B_\theta^2 = |\nabla\psi|^2/R^2$ and that of the total field $B^2 = B_\phi^2 + B_\theta^2$). Note that for the poloidal flux convention employed in [4], where spatial derivatives of ψ and derivatives of flux functions all change sign, every term in equation (9) changes sign, so that, apart from the omitted factor of 2π, the same result, including the sign, is obtained here thanks to the sign reversal in equation (5). As a consistency check, expression (9) was first evaluated in the straight cylinder plasma limit $R \to \infty$ where the Grad-Shafranov equation

$$-\frac{\partial^2\psi}{\partial R^2} + \frac{1}{R}\frac{\partial\psi}{\partial R} - \frac{\partial^2\psi}{\partial Z^2} = \mu_0 R^2 p'(\psi) + FF'(\psi) \tag{10}$$

simplifies to (ψ is now the poloidal flux per unit length and $(R, \phi, Z) \to (x, z, y)$)

$$-\frac{\partial^2\psi}{\partial x^2} - \frac{\partial^2\psi}{\partial y^2} = \mu_0 \frac{d}{d\psi}\left(p(\psi) + \frac{B_z^2(\psi)}{2\mu_0}\right) \tag{11}$$

and the general expression (9) for local shear simplifies to

$$S_\ell^{R\to\infty} = \frac{B_z}{B_\theta^2 B^2}\left\{(\psi_{xx} - \psi_{yy})(\psi_x^2 - \psi_y^2) + 4\psi_x\psi_y\psi_{xy}\right\} - \frac{B_z' B_\theta^2}{B^2}. \tag{12}$$

For an arbitrary circular plasma equilibrium with poloidal flux $\psi(r)$ and toroidal field $B_z(\psi)$, expression (12) further reduces to

$$S_\ell(r) = \frac{-B_z' B_\theta^2 + B_z(B_\theta/r - dB_\theta/dr)}{B_z^2 + B_\theta^2} \tag{13}$$

where $\boldsymbol{B}_\theta = -d\psi(r)/dr\,\hat{\boldsymbol{e}}_\theta$ for cylindrical coordinates (r, θ, z) and the magnetic axis is located at $r = 0$. The corresponding substitutions in the expression s/qR yield

$$\frac{1}{qR}\frac{r}{q}\frac{dq}{dr} = \frac{-B_z' B_\theta^2 + B_z(B_\theta/r - dB_\theta/dr)}{B_z^2} \tag{14}$$

which agrees with $S_\ell(r)$ in the approximation $B_\theta^2 \ll B_z^2$ used to obtain equation (7).

2.2. Normal and geodesic curvature

The curvature of a field line is given in terms of the parallel unit vector $\boldsymbol{b}$:

$$\boldsymbol{\kappa} = (\boldsymbol{b}\cdot\nabla)\boldsymbol{b} \equiv -\boldsymbol{b}\times\nabla\times\boldsymbol{b}. \tag{15}$$

Resolving $\boldsymbol{\kappa}$ normal and tangential to the magnetic surface we obtain the *normal curvature*: $\kappa_n = \boldsymbol{\kappa}\cdot\boldsymbol{e}_\psi$ and the *geodesic curvature*: $\kappa_g = \boldsymbol{\kappa}\cdot(\boldsymbol{b}\times\boldsymbol{e}_\psi)$. Evaluation of

equation (15) for $\boldsymbol{b} = (-\psi_Z\,\hat{\boldsymbol{e}}_R,\, F\,\hat{\boldsymbol{e}}_\phi,\, \psi_R\,\hat{\boldsymbol{e}}_Z)/(RB)$ results in the following expressions for the curvatures κ_n and κ_g in terms of standard equilibrium quantities:

$$\kappa_n = \frac{F^2\psi_R + R(\psi_{RR}\psi_Z^2 + \psi_R^2\psi_{ZZ} - 2\psi_R\psi_{RZ}\psi_Z)}{R^4 B_\theta B^2} \tag{16}$$

$$\kappa_g = \frac{-F\left[R(\psi_{RZ}(\psi_R^2 - \psi_Z^2) - \psi_R\psi_Z(\psi_{RR} - \psi_{ZZ})) + \psi_z R^2 B^2\right]}{R^5 B_\theta B^3} \tag{17}$$

The corresponding expressions in the straight cylinder limit are given by

$$\kappa_n^{R\to\infty} = \frac{\psi_{xx}\psi_y^2 + \psi_{yy}\psi_x^2 - 2\psi_{xy}\psi_x\psi_y}{B_\theta B^2}, \tag{18}$$

$$\kappa_g^{R\to\infty} = \frac{-B_z\left[\psi_{xy}(\psi_x^2 - \psi_y^2) - \psi_x\psi_y(\psi_{xx} - \psi_{yy})\right]}{B_\theta B^3}. \tag{19}$$

For an arbitrary circular equilibrium with poloidal flux per unit length $\psi(r)$ and toroidal field $B_z(\psi)$, expressions (18) and (19) reduce to

$$\kappa_n(r) = -\frac{B_\theta^2}{rB^2}; \qquad \kappa_g(r) = 0 \tag{20}$$

so that in this case the geodesic curvature vanishes, in agreement with the well-known result that magnetic field lines on circular cylindrical flux surface are geodesics and the curvature vector here is given by $\boldsymbol{\kappa} = \kappa_n\hat{\boldsymbol{e}}_r$.

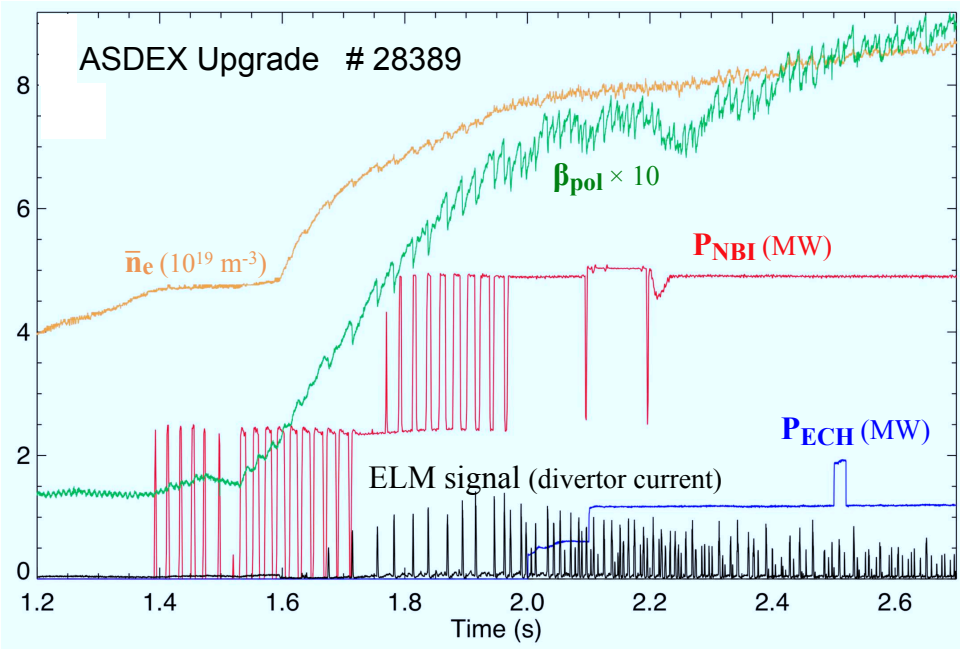

Figure 1. (colour online) Line-averaged density (ochre), poloidal beta (green), neutral beam (red) and electron cyclotron (blue) heating powers and the divertor current ELM signal (black) for ASDEX Upgrade discharge 28389 ($I_p = 1\,\mathrm{MA}$, $B_t = -2.5\,\mathrm{T}$, $\bar{n}_e = 8.9\times10^{-19}\,\mathrm{m}^{-3}$) for $1.2\,\mathrm{s} \le t \le 2.7\,\mathrm{s}$. The first ELM occurs at $t = 1.676\,\mathrm{s}$.

3. Experimental examples from ASDEX Upgrade

As an illustration, we present contour plots of the local shear for ASDEX Upgrade standard H-mode discharge 28349 ($I_p = 1\,\mathrm{MA}$, $B_t = -2.5\,\mathrm{T}$, $\bar{n}_e = 8.9 \times 10^{-19}\,\mathrm{m}^{-3}$) for which the evolution of relevant parameters in the current flat-top time window $1.2\,\mathrm{s} \leq t \leq 2.7\,\mathrm{s}$ is plotted in figure 1.

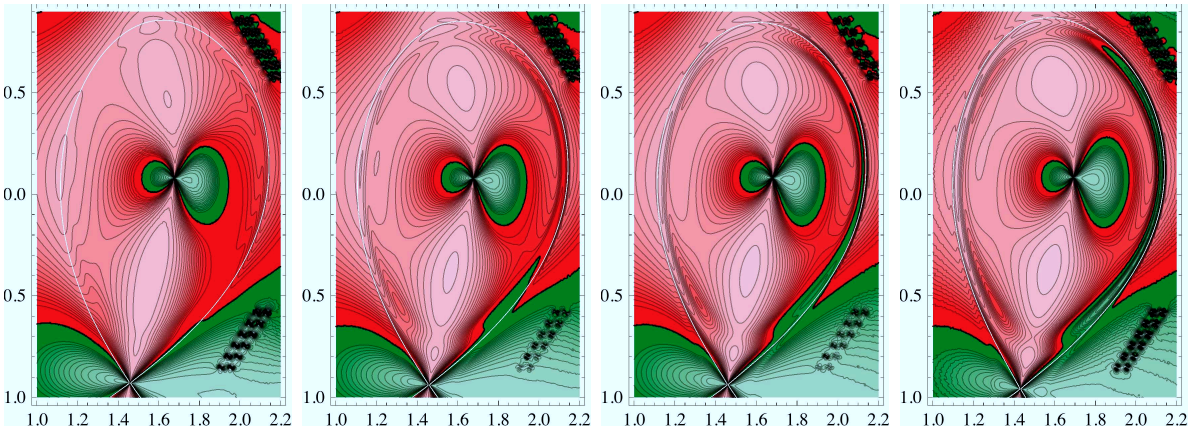

Figure 2. (colour online) Sequence of local shear contour plots for ASDEX Upgrade discharge 28389 for (left to right) $t = 1.40\,\mathrm{s}$, $t = 1.62\,\mathrm{s}$, $t = 1.70\,\mathrm{s}$, $t = 2.62\,\mathrm{s}$ calculated from CLISTE equilibrium reconstructions. These time points correspond to ohmic, pre-first ELM, post-first ELM and during a well-heated phase of the discharge (see figure 1). Red indicates negative and green positive local shear, and the darkest hues occur at zero crossings. The separatrix is plotted as a white curve. See text for more details.

Figure 2 shows a sequence of contour plots of $S_\ell(R, Z)$ evaluated using equation (9) from a sequence of equilibria constrained by equilibrium magnetic data, divertor tile current measurements, edge kinetic profiles and axial safety factor ≈ 1.0 using the CLISTE equilibrium reconstruction code [6, 7]. Each time point was selected to be at the end of the ELM recovery phase [8]. The first time point at $t = 1.4\,\mathrm{s}$ lies in the ohmic phase of the discharge, The second, at $t = 1.62\,\mathrm{s}$ is $\approx 50\,\mathrm{ms}$ before the first ELM. The third, at $t = 1.70\,\mathrm{s}$ is 25 ms after the first ELM (but before the second) and the fourth time point, $t = 2.62\,\mathrm{s}$, lies in a well-heated phase of the discharge ($\beta_{pol} \approx 0.86$). To highlight zero-crossings, the function plotted is of the form $y = \mathrm{Tanh}(1/x)$ which has a step discontinuity (jumping from $y = -1$ to $y = +1$) at $x = 0$. Here, $x \propto S_\ell(R, Z)$ with a constant of proportionality chosen to give good contrast in the contour plots. Red regions indicate negative and green positive local shear, and because of the choice of plotting function the darkest hues occur at zero crossings while the lightest occur at extrema. (Local shear is predominantly negative in the plasma because the toroidal field direction is opposite to that of plasma current flow.) The separatrix is plotted in white. The two sets of regularly spaced dark blobs near the bottom and top right-hand corners of each plot are at the locations of the lower and upper arms of the in-vessel passive conductor in ASDEX Upgrade, where for purposes of equilibrium calculations each arm is modelled by 12 wire currents.

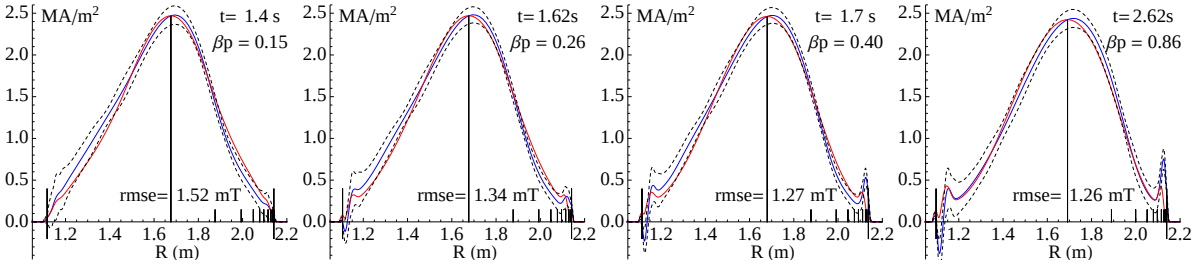

Figure 3. (colour online) Sequence of current density profiles corresponding to the contour plots in figure 2 consisting of local j_ϕ (blue) and flux surface averaged $\langle j_\phi \rangle$ (red) profiles as a function of major radius along the magnetic midplane as reconstructed by CLISTE from a combination of magnetic and edge pressure data for ASDEX Upgrade discharge # 28389. The magnetics fit errors displayed in each plot equate to $\approx 1.1\%$ of the root mean squared signal magnitude. The black dashed profiles are $\pm 1\sigma$ confidence bands for j_ϕ. The magnetic axis position and the inboard and outboard points of intersection with the separatrix are marked by vertical lines. The prominent vertical marks just above the horizontal axis on the outboard side indicate the positions of nine internal knots used in the spline parameterization of the $p'(\psi)$ and $FF'(\psi)$ source profiles for equilibrium reconstruction. The knots are concentrated in the pedestal region where the pressure data are located.

The most striking feature of the plot sequence is the growth with β_{pol} of a narrow radial region of positive shear just inside the outboard separatrix. Starting in the lower outboard quadrant, the positive shear region first crosses the midplane at a time separated by the order of 10 ms from the occurrence of the first ELM, a pattern that has been systematically observed in ELMy discharges by plotting the magnetic midplane profile of S_ℓ which is a standard output of CLISTE. With increasing β_{pol}, the region of positive S_ℓ broadens radially and extends poloidally upwards, while remaining confined to the outboard side. This correlates with the growth in the outboard peak in the toroidal current density profile shown in the corresponding sequence in figure 3.

The asymmetric figure-of-eight region of positive shear centered on the magnetic axis and present on all plots can be shown to be a consequence of ellipticity as follows: Consider the straight cylinder equilibrium $\psi(x,y) = \psi_0(1 - (ax^2 + by^2)/2)$ with elongation everywhere given by $k = \sqrt{a/b}$ and positive, constant current density $j(x,y) = (a+b)\psi_0/\mu_0$ where we choose $B_z(\psi) = B_0\sqrt{1 + 2c\,\psi/B_0^2}$ and hence $B_z' = c/B_z$. Evaluation of equation (12) yields the following expression for the local shear:

$$S_\ell(x,y) = \frac{(b-a)\psi_0 B_z}{B^2}\,\frac{a^2x^2 - b^2y^2}{a^2x^2 + b^2y^2} - \frac{c\,\psi_0^2(a^2x^2 + b^2y^2)}{B_z B^2} \tag{21}$$

where $B^2 = B_z^2 + B_\theta^2 = B_z^2 + \psi_0^2(a^2x^2 + b^2y^2)$. For $k = 1$, i.e. $a = b$ the first term vanishes and the second is a function of $r^2 = x^2 + y^2$ and hence contours of S_ℓ in this case are concentric circles. By contrast, the left-hand plot in figure 4 shows contours of $S_\ell(x,y)$ for $k = 1.5$, $B_0 = -1$ and $c = 0$ (thus B_z is constant). Here, the asymptotes $y = \pm k^2 x$ divide unbounded regions of positive and negative local shear; $b < a$ and $(b-a)\psi_0\, B_z > 0$, hence S_ℓ is positive for $a^2x^2 > b^2y^2$ and negative for $a^2x^2 < b^2y^2$. In

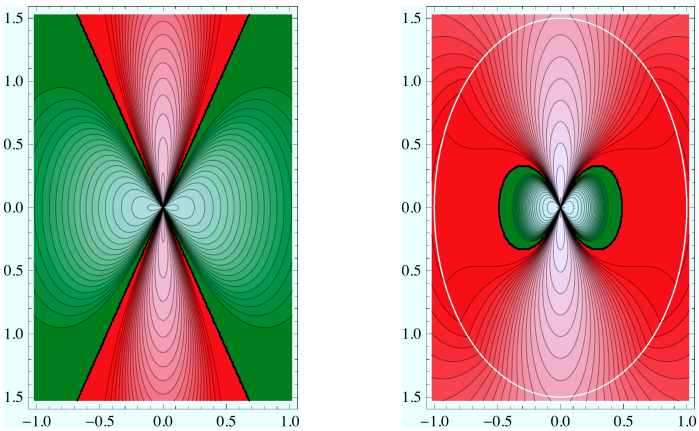

Figure 4. Contour plots of local shear S_ℓ for the straight cylinder equilibrium $\psi(x,y) = (1-(x^2+(2y/3)^2)/2)$ with (left plot) constant $B_z = -1$ and (right plot) $B_z = -\sqrt{1-.35\psi}$. The figure-of-eight positive shear region present in figure 2 is reproduced in symmetric form in the right-hand plot.

the right-hand plot, $c = -0.35$, $B_z = -\sqrt{1-0.35\,\psi}$ and, along the midplane $y = 0$, the negative second term in equation (21) dominates the positive first term for $|x| \gtrsim 0.5$ which results in a finite region of positive local shear similar to the figure-of-eight pattern present in figure 2. In contrast to figure 2, the pattern here is both up-down and in-out symmetric since $S_\ell(x,y)$ is an even function of both x and y.

Given the pattern of local shear reversal in the pedestal region at the occurrence of the first ELM, it is interesting to consider the corresponding behaviour of the poloidal current density profile, recently proposed as a critical quantity in discriminating between plasma regimes [9, 10] and as a mechanism for phase transitions [11]. CLISTE output includes error bars for the fitted $p'(\psi)$ and $FF'(\psi)$ source profiles calculated from the variance-covariance matrix of the linear regression which determines the set of free parameters at the cycle where the convergence criterion is met [7]. Error bars for related quantities such as the poloidal current density profile $j_\theta = F'B_\theta/\mu_0$ are easily constructed. Figure 5 shows the outboard magnetic midplane profile $j_\theta\,(R,\ Z_{mag.\,axis})$ with 1σ error bars (blue traces) for the four time points in figures 2 and 3. Also plotted (red trace) is the local shear midplane profile $S_\ell\,(R,\ Z_{mag.\,axis})$. The evolution of the two profiles is closely correlated, in particular the S_ℓ profile increases through zero at the same radial location, within 1σ error bars, as j_θ for the post-first ELM time points $t = 1.7\,\mathrm{s}$ and $t = 2.62\,\mathrm{s}$. Note that j_θ is already weakly positive for the pre-first ELM time point $t = 1.62\,\mathrm{s}$. In this discharge, the L-H transition occurs at $t = 1.59\,\mathrm{s}$ but a systematic study of the correlation of the L-H transition with the zero crossing of j_θ has not been attempted here and instead will form the subject of a future publication. The last term in equation (9) for S_ℓ has a direct dependence on j_θ through the presence of the factor F' and hence it might be assumed that this term explains the similar evolution of j_θ and S_ℓ. Its magnitude, however, is negligible in the pedestal region

($|F'B_\theta^2/B^2| \approx 0.01$) and instead it is the temporal evolution of ψ_{RR} that determines the development of the sign reversal in S_ℓ in the pedestal, as can be seen from the green and magenta traces in figure 5 which represent a partitioning of S_ℓ into the ψ_{RR} - dependent term $(F/(R^4B_\theta^2B^2))\psi_{RR}(\psi_R^2 - \psi_Z^2)$ (green trace) and all other terms in equation (9) (magenta trace). Both traces are monotonic in the pedestal region for the ohmic time point $t = 1.4\,\mathrm{s}$. Thereafter the magenta trace, which includes the term $-F'B_\theta^2/B^2$, remains almost monotonic, but the green trace develops a prominent local maximum 2 cm inside the separatrix which accounts for the sign reversal in S_ℓ.

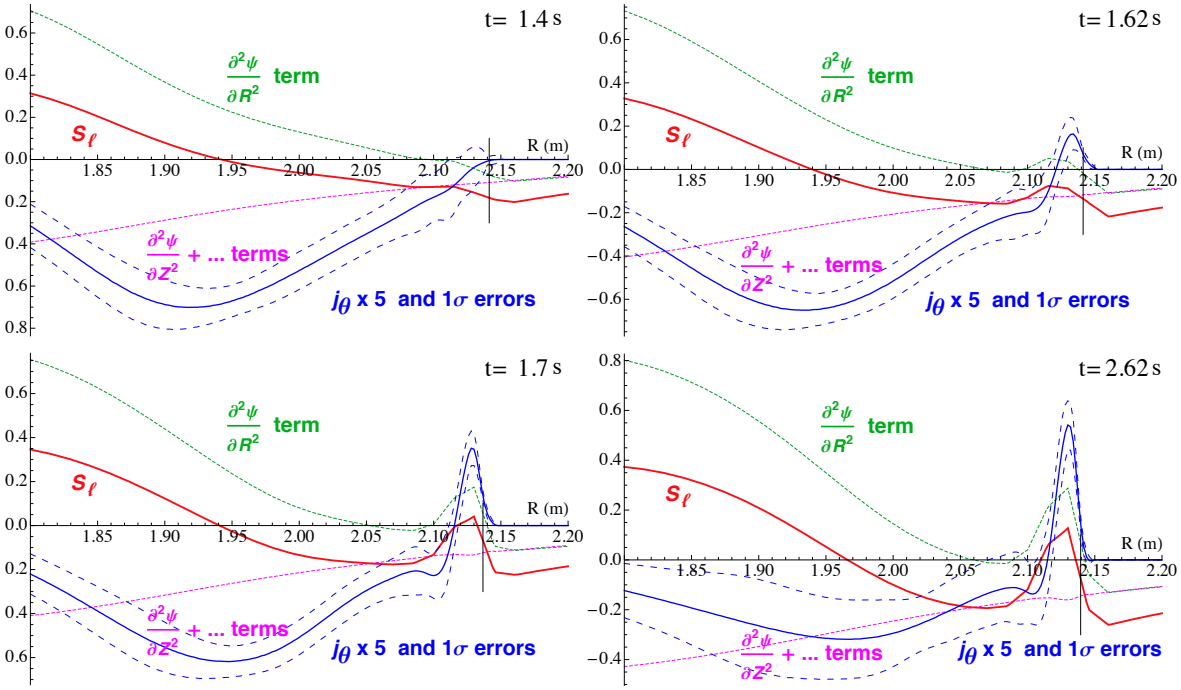

Figure 5. (colour online) Sequence of outboard magnetic midplane profiles of local shear components (units: m^{-1}) and scaled poloidal current density (units: $\mathrm{MA/m}^2$) versus major radius for ASDEX Upgrade discharge 28389 and the time points shown in figure 2. The green dotted trace is the expression $(F/(R^4B_\theta^2B^2))\psi_{RR}(\psi_R^2 - \psi_Z^2)$. The magenta trace consists of all other terms in equation (9). The red trace, the sum of the green and magenta traces, is the local shear. The blue traces consist of the poloidal current density (solid) and 1σ error bars (dashed). The black vertical line at $R \approx 2.14\,\mathrm{m}$ marks the separatrix location.

4. Summary

An exact relation for axisymmetric equilibria of arbitrary cross-section has been derived for the local magnetic shear defined in equation (5) in terms of the poloidal flux per radian ψ and its spatial derivatives, and the flux function $F(\psi) = RB_\phi$ and its flux derivative F'. Similar expressions for the normal and geodesic curvature have also been derived. These practical formulae are easily evaluated using standard equilibrium code output quantities. Initial application of the local shear expression to ASDEX Upgrade

equilibrium reconstructions with the CLISTE code reveal systematic local shear reversal in the outboard pedestal region which first appears at a time very close to that of the first ELM, and is accompanied by a zero crossing of the poloidal current density close to the same location. The correlation in the evolution of j_θ and S_ℓ in the pedestal region is not trivially explained by the presence of $j_\theta = F' B_\theta / \mu_0$ in equation (9). This preliminary experimental finding of a strong temporal correlation between local shear reversal in the pedestal, a zero crossing of the poloidal current density and the appearance of the first ELM merits further careful investigation which will form the subject of a future publication.

5. Acknowledgments

This work was supported by a research agreement between the Max Planck Institut für Plasmaphysik, Garching and the Department of Physics, University College Cork, and by EURATOM.

References

[1] J M Greene and J L Johnson, Plas. Phys. **10**, 729 (1968).
[2] J M Greene and M S Chance, 1981 Nucl. Fusion **21** 453 (1981).
[3] J L V Lewandowski and M Persson, Plas. Phys. Control. Fusion, **37** 1199 (1995).
[4] M Nadeem, T Rafiq and M Persson, Phys. Plas, **8** 4375 (2001).
[5] Wolfram Research, Inc., Mathematica, Version 8.0, Champaign IL, (2010).
[6] P J Mc Carthy, Phys. Plas. **6** 3554 (1999).
[7] P J Mc Carthy and ASDEX Upgrade Team, Plasma Phys. Control. Fusion **54** 015010 (2012).
[8] M G Dunne et al., Nucl. Fusion **52** 123014 (2012).
[9] J Garcia and G Giruzzi, Phys. Rev. Lett. **204** 205003 (2010).
[10] J Garcia and G Giruzzi, Plasma Phys. Control. Fusion **54** 015009 (2012).
[11] E R Solano and R D Hazeltine, Nucl. Fusion **52** 114017 (2012).